Proceedings of GT2007
ASME Turbo Expo 2007: Power for Land, Sea and Air
May 14-17, 2007, Montreal, Canada

GT2007-27800

THREE-DIMENSIONAL VISCOUS FLUTTER ANALYSIS OF STANDARD CONFIGURATION 10

Paul J. Petrie-Repar*
RPMTurbo
7 Havana St
Ashgrove, Queensland, 4060
Australia
Email: Paul.Petrie-Repar@rpmturbo.com

Andrew McGhee
RPMTurbo
7 Havana St
Ashgrove, Queensland, 4060
Australia

Peter A. Jacobs
Mechanical Engineering Department
University of Queensland
St Lucia, Queensland, 4072
Australia

ABSTRACT

The results of a three-dimensional (3D) viscous flutter analysis for a compressor stage, Standard Configuration 10, are presented. The unsteady flow simulations were performed by a 3D linearized Navier-Stokes flow solver using the Spalart and Allmaras turbulence model. Significant flow blockage due to corner separation at the hub on the suction surface was predicted by the steady-state 3D viscous simulation at a design condition. Corner separation was not predicted by 3D inviscid or two-dimensional (2D) viscous simulations. The corner separation was found to have a destabilizing effect and changed the nature of the unsteady flow. In fact, the 3D viscous simulations predicted negative aerodynamic damping for almost half of the inter-blade phase angles, while the 2D and 3D inviscid simulations predicted stable positive aerodynamic damping for all inter-blade phase angles. An off-design flow condition was also examined and significant differences between the 2D and 3D viscous simulations were found.

NOMENCLATURE

β_1 tangential flow angle at inlet
σ interblade phase-angle
ω^* reduced frequency based on full chord
f blade vibration frequency
M_1 inlet Mach number
y^+ non-dimensional distance from wall
NRBC non-reflecting boundary condition

INTRODUCTION

Blade flutter is a significant problem for the manufacturers of large-scale turbomachinery such as gas turbines, steam turbines and aircraft engines. It can lead to dramatic blade loss in the short-term and high-cycle fatigue (HCF) in the long-term. The occurrence of blade flutter has a significant economic cost due to increased development costs, losses due to development delays, maintenance costs, and losses due to downtime. It has been estimated that 30 percent of overall development costs of jet engines is due to HCF management and that each new jet engine development has on average 2.5 HCF problems which lead to considerable time delays and cost overruns [1]. Delays in development for a medium-size 500 MW power plant can lead to a loss of revenue up to $2.5 million US dollars (1996) per week [2].

Flutter is self-excited vibration of a structure due to the interaction of structural-dynamic and aerodynamic forces. For most turbomachinery cases, the structural forces dominate. Hence, the aerodynamic forces can be neglected when determining the mode shapes of the blade motion. Also, the unsteady aerodynamic response can be determined with the assumption that the blade motion is known *a priori*. The flutter risk is then assessed by calculating the work done by the unsteady aerodynamic forces on the blades.

The most difficult and computationally expensive compo-

*Address correspondence to this author.

Copyright © 2007 by RPMTurbo Pty Ltd

nent of flutter prediction is the determination of the unsteady aerodynamic forces. Flutter usually occurs at off-design operating conditions where flow separation occurs. In order to accurately predict separated flow, 3D viscous flow modelling is necessary. In the past, 3D unsteady viscous flow modelling has been too computationally expensive to use during the design phase because hundreds of different cases (various operating points and modes) have to be examined. Manufacturers have had to rely on simplified flow models (e.g. 2D inviscid), reduced order models and empirical data during the design process and 3D viscous flutter analysis was only for research purposes. However, due to the continuing development of numerical methods and the constant increase in the speed and memory of computer hardware, it is now possible to perform 3D viscous flutter analysis during the design phase. For example, the numerical method employed to perform simulations for this paper, is capable of performing an unsteady 3D viscous simulation in 20 minutes.

Design engineers need to have a good understanding of the capabilities and limitations of a numerical method. This can be achieved by comparing solutions from the numerical method with analytical solutions, the results from other numerical methods and experimental data. While comparison with experimental data is essential for determining whether a flow model is adequate for a particular case, it is not possible to determine whether a numerical method is solving the governing equations correctly by comparing solutions with experimental data. This can only be achieved by comparing solutions with analytical solutions and solutions from independently developed numerical methods. Also, it is not possible to evaluate a flow model if the numerical method is not solving the governing equations correctly.

Analytical solutions only exist for simple geometries and uniform flow conditions. However, the ability of a numerical method to solve the governing equations accurately for real profiles can be assessed by comparing solutions with other numerical methods that solve the same governing equations. A comprehensive database of 2D solutions for unsteady flow through vibrating turbomachine-cascades has been established [3]. However, solutions to 3D Standard Configurations are scarce.

Montgomery and Verdon [4] proposed a 3D Standard Configuration 10 test case and performed 3D inviscid unsteady flow simulations for the new test case. Unsteady inviscid flow simulations of this test case have also been performed by Kemme [5] in the time-domain and Poli *et al.* [6] in the frequency domain. As far as the author is aware, all previous investigations of this 3D configuration have only been inviscid.

Recently Vogt [7] published experimental data for a 3D low pressure turbine. The turbine geometry and experimental data have been fully described. The experimental data was compared with solutions from 3D unsteady inviscid flow simulations that included tip clearance.

Rzadkowski *et al.* [8] has published results from 3D unsteady viscous simulations of Standard Configuration 11, a 2D turbine profile, and compared the results with experimental data.

The unsteady flow solutions presented in this paper were calculated by a 3D linearized Navier-Stokes method. The ability of linearized Navier-Stokes methods to predict unsteady flow with separated flow regions has been previously demonstrated. Clark & Hall [9] achieved a good agreement between predictions from a linearized 2D Navier-Stokes method and experimental data from a low-speed (inlet Mach number 0.2) off-design flow condition for a fan blade. Sbardella & Imregun [10] compared linearized 3D viscous/inviscid solutions with experimental data for a transonic off-design condition of a 2D turbine test case. While there were discrepancies between the computed and experimental data, the linearized viscous solution was closer to the experimental data than the linearized inviscid solution.

In this paper the results of 3D unsteady viscous simulations of Standard Configuration 10 are presented. Two operating conditions are examined: an on-design and one off-design condition. The results are compared with 3D inviscid and 2D simulations and the differences are discussed. The results also establish a database of computational solutions which are available to other researchers for comparison. The results shown here are available for download from www.rpmturbo.com/testcases/sc10_3D.

NUMERICAL METHOD

The steady-state and unsteady flow simulations presented here were performed by RPMTurbo's in-house flow solvers. The unsteady flow simulations were calculated by a linearized flow method based on the steady-state method. The steady-state method and the linearized flow method solve the full 3D steady-state and linearized Reynold's averaged Navier-Stokes equations using the Spalart and Allmaras turbulence model [11] (no transition model) over the entire flow domain (no thin-layer approximation).

The verification of the ability of the numerical method to solve the 2D Euler and Navier-Stokes equations has been presented previously [12].

The main feature of the linearized flow solver is the efficient manner in which it can solve the linearized 3D unsteady viscous flow equations. For example it can solve a 3D viscous problem on a mesh with 455 988 cells in 20 minutes using 35 processors. This is approximately 1000 times faster than conventional time-marching methods for the same problem. This makes it possible to analyze hundreds of cases in a time frame that is acceptable to design engineers.

A one-dimensional non-reflecting boundary condition (1D-NRBC) was applied at the far-field (inlet and outlet) for the 3D simulations presented here. This boundary condition assumes that the unsteady waves at the far-field are planar and the wave fronts are perpendicular to the axial direction. This is only true when the inter-blade phase angle is zero. The 2D-NRBC of Giles [13] has been implemented in the current method but can

Copyright © 2007 by RPMTurbo Pty Ltd

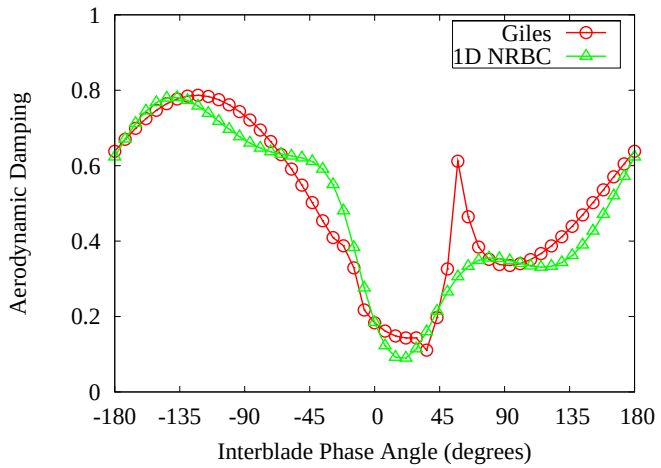

Figure 1. 2D STANDARD CONFIGURATION 10: AERODYNAMIC DAMPING AT SUBSONIC FLOW CONDITION DUE TO TORSION MODE ($\omega^* = 0.5$) CALCULATED WITH 1D AND 2D NRBC.

only be applied to 2D problems. It is possible to apply 2D-NRBC in a strip-wise fashion on 3D problems, however, this has not been implemented in the current method. The authors are currently attempting to implement an exact 3D-NRBC method. The resulting error from the application of the 1D-NRBC is examined in Figure 1. Here the aerodynamic damping as a function of inter-blade phase angle for the 2D Standard Configuration 10 at a subsonic flow condition ($M_1 = 0.7$ and $\beta_1 = 55^\circ$) for a torsion mode ($\omega^* = 0.5$) is shown. Two solutions are shown: one applies the 1D-NRBC and the other applies the 2D non-reflecting boundary conditions of Giles. The 1D-NRBC fails to predict the correct damping near the resonant inter-blade phase angles which are 58.5 and -13.5 degrees at the upstream far-field and 29.8 and -15.9 degrees in the downstream far-field for this case. At resonant conditions, an acoustic wave in the far-field is planar and its wave front is parallel to the axial direction, hence the poor performance of the 1D-NRBC. It is concluded from the above result that the performance of the 1D-NRBC is satisfactory for the majority of inter-blade phase-angles that are not near the resonance.

Montgomery & Verdon [4] and Poli *et al.* [6] have presented the results of 3D inviscid simulations for Standard Configuration 10 using multidimensional NRBC. Montgomery & Verdon applied a 3D-NRBC. Poli *et al.* applied a 1D-NRBC and the 2D-NRBC of Giles in a strip-wise fashion and compared their results with Montgomery & Verdon. There was good agreement between the method of Poli *et al.* and Montgomery & Verdon. The agreement between the 1D-NRBC and the multidimensional methods was reasonable for conditions not near resonance.

Table 1. DETAIL OF 3D VISCOUS MESHES.

Mesh Resolution	Medium	High
Number of Cells	455 988	1 594 728
Cells in Radial Plane	11 692	22 149
Cells in Radial Direction	39	72
Profile $y^+_{\max}$	6.4	2.4
Profile $\overline{y^+}$	1.8	0.9
Hub/Outer Housing $y^+_{\max}$	4.1	2.3
Hub/Outer Housing $\overline{y^+}$	1.1	0.7

PROBLEM DESCRIPTION

The geometry of the 3D Standard Configuration 10 has been described by Montgomery & Verdon [4]. It consists of 24 evenly spaced straight blades. The cross-section of the blades is the same as the 2D Standard Configuration 10 test case. The leading edges of the blades are on lines which radiate out from the same point on the axis and the lines are perpendicular to axis. The radius of the hub is 3.395 chord lengths and the radius of the outer housing is 4.244 chord lengths. There is no tip clearance. For the viscous simulations, the chord length was set to 100 mm. The pitch to chord ratio is 1.0 at mid-radius.

The mode shape examined here is torsion about (0.5, 0.05) in profile co-ordinates. The mode shape does not vary with radius, and it is assumed that the blade slides over the hub and the outer housing.

Meshes

The 3D viscous simulations were performed on a medium and a high resolution multi-block mesh. The flow solvers used to perform the simulations treat the mesh as an unstructured mesh. The details of the meshes are shown in Table 1. The current numerical method solves the full Reynolds averaged Navier-Stokes equations over the entire domain (no thin layer approximation) and does not use wall functions to estimate the boundary layer. Therefore it is necessary to have several mesh points in the boundary layer with the first mesh line sufficiently close to the wall. The meshes were designed to fully resolve the boundary layer flow on the blade, and also the hub and the outer housing. The maximum and average y^+ values for the cell centers on the wall surfaces are shown in Table 1. The inlet and outlet boundaries of the meshes are located one chord length from the profile edges. The 3D inviscid simulations presented in this paper were performed on an unstructured mesh of 89055 hexahedral cells with 15 cells in the radial direction.

Copyright © 2007 by RPMTurbo Pty Ltd

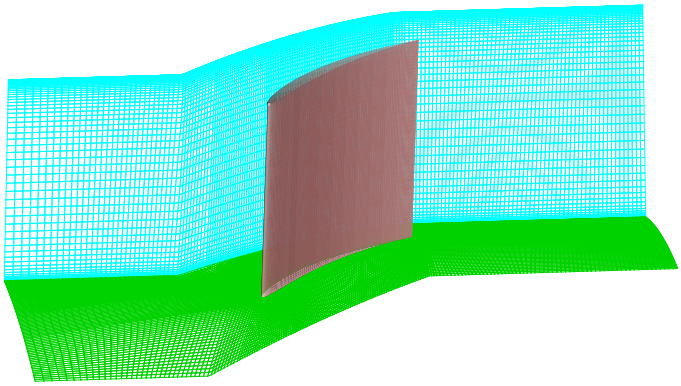

Figure 2. HIGH RESOLUTION MESH FOR 3D STANDARD CONFIGURATION 10.

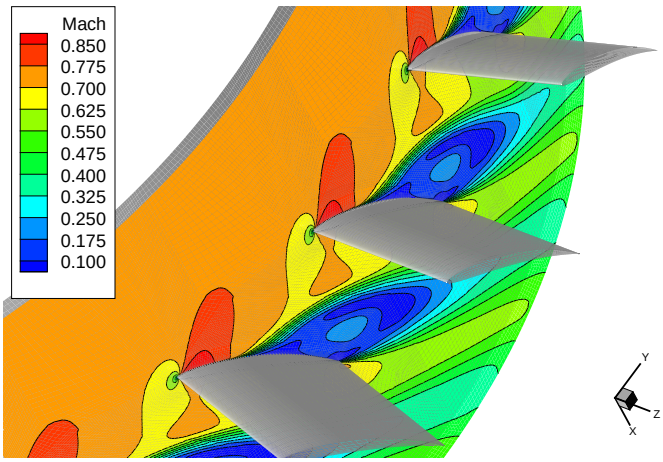

Figure 3. CONTOUR PLOT FLOW MACH NUMBER AT 10 % BLADE HEIGHT FOR 3D STANDARD CONFIGURATION 10.

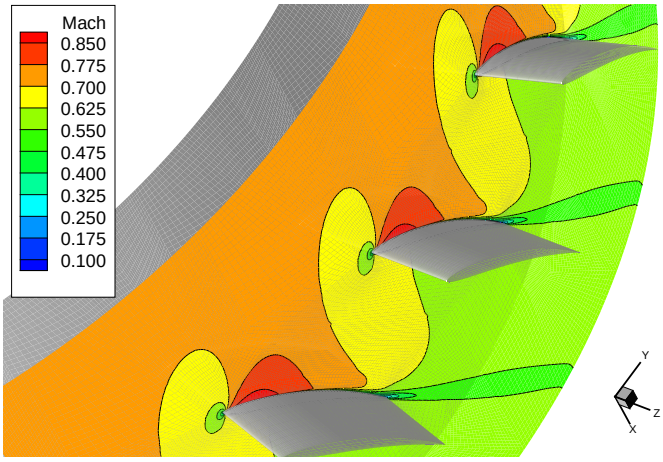

Figure 4. CONTOUR PLOT FLOW MACH NUMBER AT 50 % BLADE HEIGHT FOR 3D STANDARD CONFIGURATION 10.

RESULTS

In this paper two operating points are examined. Firstly, a design operating point, which is the same as the subsonic condition defined for the 2D Standard Configuration 10, is examined. Secondly, an off-design operating point at a higher inlet Mach number near stall is examined.

Design Operating Point

The design operating point is defined as $M_1 = 0.7$ and $\beta_1 = 55^\circ$. For the viscous simulations the total pressure was 101.3 kPa and the total temperature was 300 K. The prescribed flow conditions were assumed to be uniform at the far-field boundaries. The Reynolds number for this condition is 1.26×10^6. The flow condition examined here is different from that examined by Montgomery and Verdon [4] and Kemme [5]. They assumed that the blades were rotating and that the tangential flow angle at the inlet in the stationary frame of reference was zero. They assumed that the rotation speed was such that the tangential flow angle at mid-radius in the rotating frame of reference was 55.0 degrees. As a result, the inlet tangential flow angle was 51.8 degrees at the hub and 57.8 degrees at the outer housing for the inviscid 3D simulations performed by Kemme and Montgomery. The inlet flow angle for the original 2D test case is defined as a constant 55 degrees. Viscous 2D steady-state solutions for the inlet flow angles at the hub and the housing used by Montgomery (and inlet Mach number 0.7) are near the separated flow boundary [12]. Note that the proximity of the flow condition at the end walls to the separated flow boundary was not an issue for Montgomery as his simulations were inviscid. It was decided to set the inlet flow angle to be a constant 55 degrees at all radii and to assume that the blades are not rotating for the viscous 3D simulations presented here. This was done to demonstrate that the flow separation was due to the presence of the viscous boundary at the hub and not due to the incident flow angle.

The contour plots of flow Mach number at 10% and 50% blade heights are shown in Figures 3 and 4 respectively. A significant region of the flow-field at 10% blade height near the suction surface and trailing edge has a flow Mach number less than 0.3. This is due to corner separation, which can clearly be seen in the stream-trace plot on the hub and the profile shown in Figure 5. The corner separation causes a significant flow blockage which was not predicted by the 2D or the 3D inviscid simulations. As a result, a significantly lower exit pressure was required for the 3D viscous simulation to achieve $M_1 = 0.7$. The exit pressures required for the various flow models are shown in Table 2.

The isentropic Mach number on the blade surface at 10%

Copyright © 2007 by RPMTurbo Pty Ltd

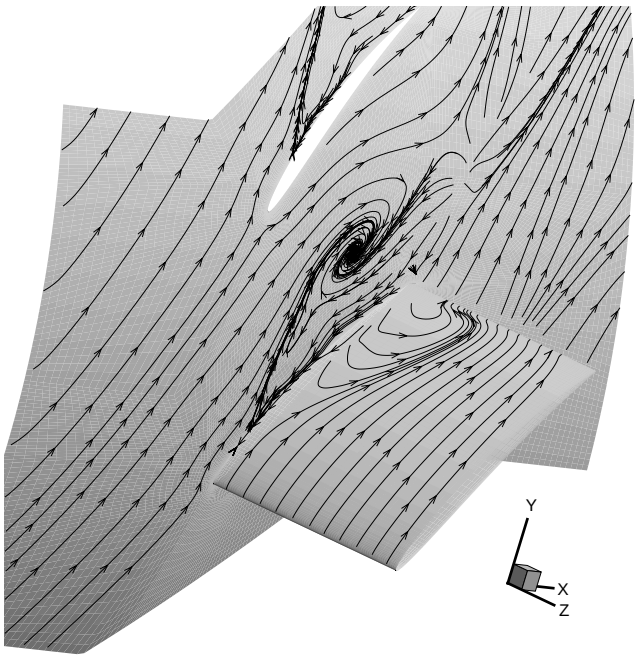

Figure 5. STREAM-TRACE ON HUB AND PROFILE FOR 3D STANDARD CONFIGURATION 10 AT DESIGN OPERATING POINT.

Table 2. AVERAGE EXIT PRESSURE REQUIRED TO ACHIEVE FLOW MACH NUMBER 0.7 AT INLET.

Flow Model	Exit Pressure (kPa)
2D Viscous	87.26
3D Inviscid	87.62
3D Viscous	81.20

and 50% blade heights is shown in Figures 6 and 7 respectively. The 3D inviscid and 2D solutions presented in this paper were also calculated by RPMTurbo's in-house flow solvers. Though not shown here, the 2D viscous and 2D inviscid solutions are very similar for this condition [12]. There is good agreement between the 3D inviscid the 2D solutions at 50% blade height. Montgomery & Verdon and Kemme also found good agreement for this condition even though their inlet tangential flow angle did vary with blade height. There is a small difference between the 3D inviscid and the 2D solutions at 10% blade height with the peak flow Mach number slightly higher for the 3D inviscid result near the leading edge. Note that the 3D inviscid solution of Montgomery for this case did vary with blade height.

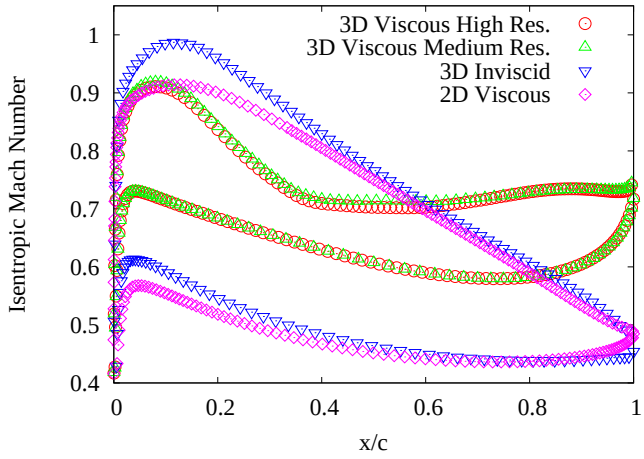

Figure 6. SURFACE ISENTROPIC MACH NUMBER AT 10 % BLADE HEIGHT FOR 3D STANDARD CONFIGURATION 10.

There are significant differences between the 3D viscous and the other (3D inviscid and 2D) flow solutions. The isentropic Mach number at the trailing edge at both blade heights is significantly higher for the 3D viscous solution. This is due to the flow blockage caused by the corner separation. The exit pressure required at outlet for the 3D viscous simulation is significantly lower in order to match the inlet Mach number. Hence the pressure at the trailing edge is lower and the isentropic Mach number is higher. The shape of the isentropic Mach number plot at 10% blade height for the 3D viscous solution is significantly different because of flow separation at 40% chord. The separated flow region can be identified in Figure 8 as the region where the friction coefficient is negative.

There is good agreement between medium and high resolution solutions for the 3D viscous solutions at both heights. It appears that the medium resolution 3D viscous mesh is resolving the flow adequately for this case.

The local work coefficient of the unsteady flow due to the torsion mode with $\omega^* = 0.5$ and $\sigma = 0^\circ$ at 10% and 50% blade heights is shown in Figures 9 and 10 respectively. Though not shown here, the 2D viscous and 2D inviscid unsteady solutions for this case are very similar [12]. There is good agreement between the 3D inviscid and 2D solutions at both blade heights for this case. This is consistent with results of Kemme and Montgomery & Verdon. Kemme found good agreement between the 2D and 3D inviscid solution for this case at mid-height. Montgomery and Verdon found good agreement between the 2D and 3D inviscid solution for this case at various blade heights (hub, middle and outer housing).

As was the case for the steady solutions, there are significant differences between the 3D viscous solutions and the other (3D inviscid and 2D) unsteady flow solutions. The local work

Copyright © 2007 by RPMTurbo Pty Ltd

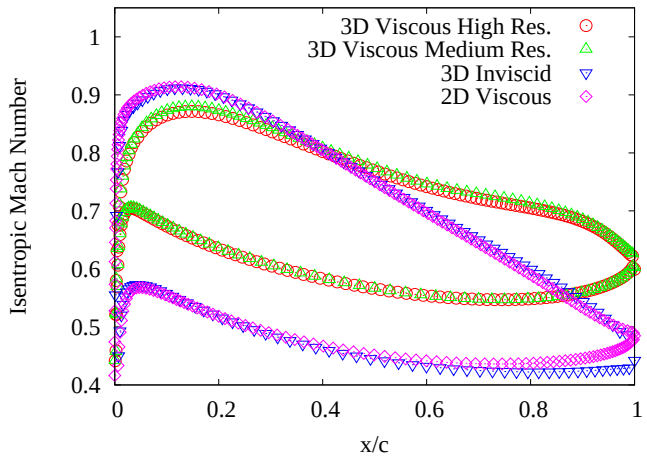

Figure 7. SURFACE ISENTROPIC MACH NUMBER AT 50 % BLADE HEIGHT FOR 3D STANDARD CONFIGURATION 10.

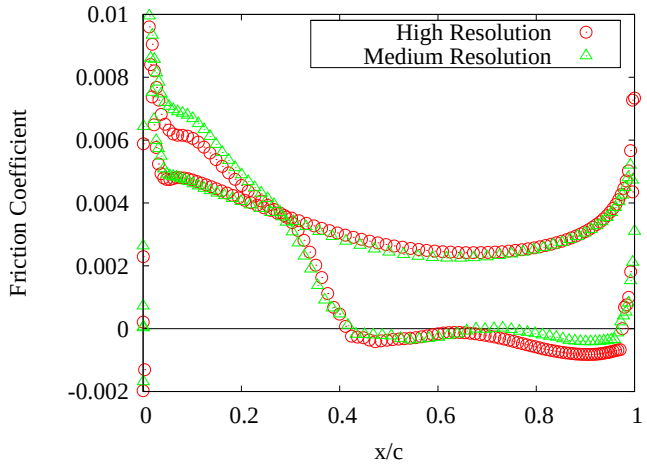

Figure 8. FRICTION COEFFICIENT AT 10 % BLADE HEIGHT FOR 3D VISCOUS SIMULATION OF STANDARD CONFIGURATION 10.

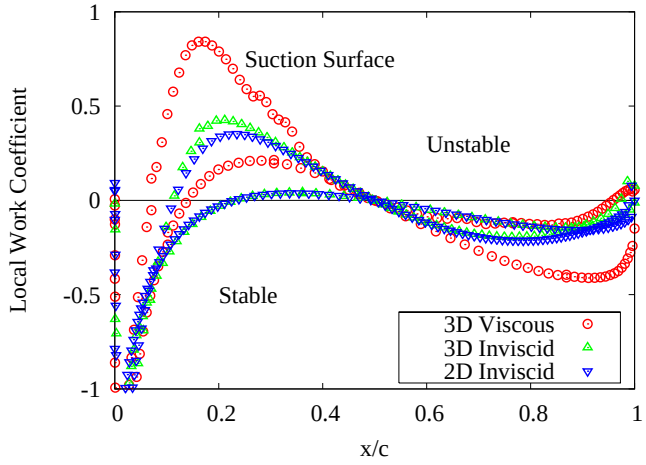

Figure 9. LOCAL WORK COEFFICIENT FOR TORSION MODE AT $\sigma = 0^\circ$ AND AT 10 % BLADE HEIGHT

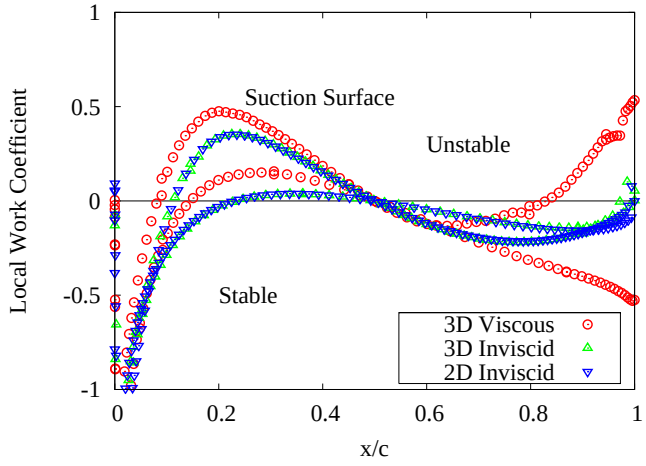

Figure 10. LOCAL WORK COEFFICIENT FOR TORSION MODE AT $\sigma = 0^\circ$ AND AT 50 % BLADE HEIGHT.

coefficient near the leading edge on both the pressure and suction surfaces is significantly more destabilizing for the 3D viscous solution at both blade heights with the effect being more pronounced at 10% blade height. Differences also exist near the the trailing edge, particularly for the 50% blade height. The differences are probably due to the fact that the flowfield near the trailing edge is different from the 3D inviscid and 2D flow-fields because of the presence of the corner separation.

The aerodynamic damping as a function of interblade phase angle for the torsion mode with $\omega^* = 0.5$ is shown in Figure 11. The aerodynamic dampings were calculated from the linearized flow solution for all inter-blade phase angles shown in this figure. Note that the 1D-NRBC was used for all simulations shown in this figure. Once again, the 3D inviscid and 2D solutions are similar and the 3D viscous solution is significantly different. The 3D inviscid and 2D solutions are stable for all interblade phase angles. However, the 3D viscous solution is unstable for $30^\circ \leq \sigma \leq 180^\circ$. The greatest difference occurs at $\sigma = 135^\circ$. The local work coefficient for interblade phase angle $\sigma = 90^\circ$ at 10% and 50% blade height is shown in Figures 12 and 13 respectively. This inter-blade phase angle was chosen to make it easier for other researchers to repeat the calculation with a time-marching method that may not have a phase-lag periodic boundary condition. The plot of local work coefficient for the 3D

Copyright © 2007 by RPMTurbo Pty Ltd

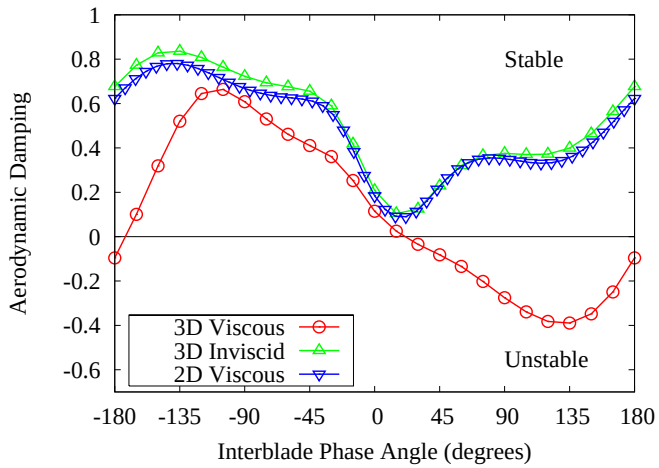

Figure 11. AERODYNAMIC DAMPING FOR 3D STANDARD CONFIGURATION 10.

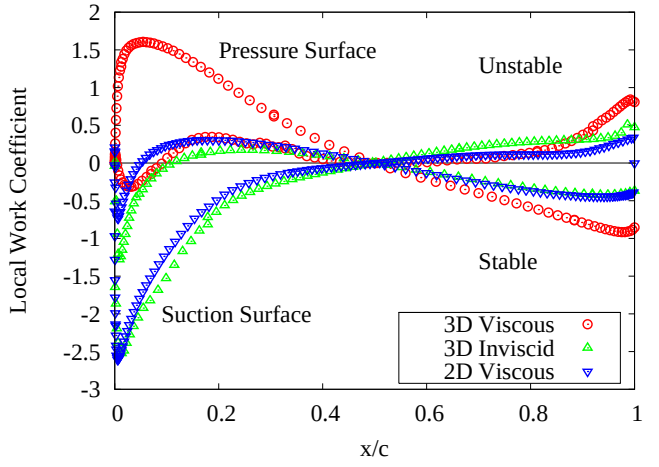

Figure 12. LOCAL WORK COEFFICIENT FOR TORSION MODE AT $\sigma = 90^\circ$ AND AT 10 % BLADE HEIGHT.

viscous solution is completely different to the other solutions for this interblade phase angle. It appears that the nature of the unsteady 3D viscous flow is very different to that predicted by the other flow models (3D inviscid, 2D) for this interblade phase.

Off-Design Flow Condition

An off-design operating point is now examined. The operating point is the same as the off-design operating point examined by the authors in a previous paper [12]. At this condition, large values of negative aerodynamic damping were predicted by 2D viscous simulations. This operating condition was chosen to de-

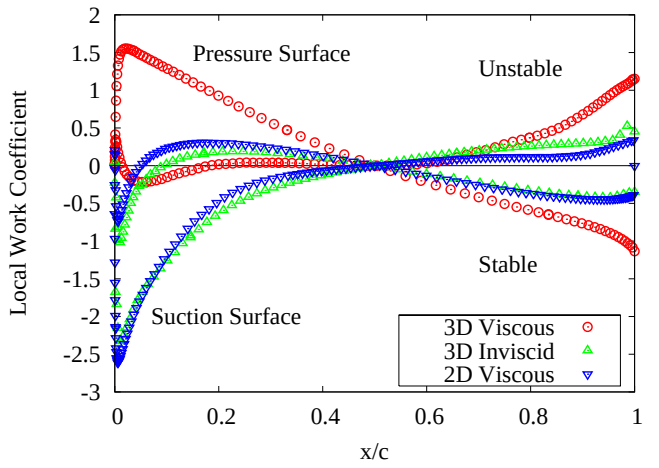

Figure 13. LOCAL WORK COEFFICIENT FOR TORSION MODE AT $\sigma = 0^\circ$ AND AT 50 % BLADE HEIGHT.

termine whether the large values of negative aerodynamic damping would be predicted by 3D viscous simulations. The operation point is defined as $M_1 = 0.81$ and $\beta = 59.0^\circ$. The Reynolds number for this condition is 1.36×10^6.

The flow-fields for 2D viscous and 3D viscous simulations are shown in Figures 14 and 15 respectively. The flow-field at mid-blade height is shown for the 3D simulation. To aid comparison, the contour levels are the same in both figures. The flow-fields differ because of the lower exit pressure for the 3D simulation due to flow blockage from corner separation. Other differences for the 3D viscous solution are: higher flow Mach number at exit, weaker expansion of the flow downstream of the leading edge on the suction surface and a smaller separated flow region near the trailing edge on the suction surface.

The aerodynamic damping as a function of interblade phase angle for the torsion mode with $f = 110.8$ Hz ($\omega^* = 0.263$) is shown in Figure 16. Two 2D viscous solutions are shown: one with 1D-NRBC and the other with the 2D-NRBC of Giles. Both 2D solutions predict large values of negative damping near $\sigma = 200^\circ$. However the inter-blade phase angle and magnitude of the minimum values do differ. This is probably due to reflections of large magnitude pressure waves at the farfield boundaries in the simulation with 1D-NRBC. The fact that both boundary conditions predict the large peak value and that the peak value occurs far away from the farfield resonances [12], suggests that the instability is due to some form of near-field resonance. It appears that 3D viscous simulations of this off-design operating point do not predict large values of negative damping as predicted by 2D viscous simulations. The magnitude of the aerodynamic damping predicted by the 3D viscous simulations is so small in comparison with the 2D viscous result that it appears to be zero in Figure 16. The magnitude of the 3D viscous aerodynamic damp-

Copyright © 2007 by RPMTurbo Pty Ltd

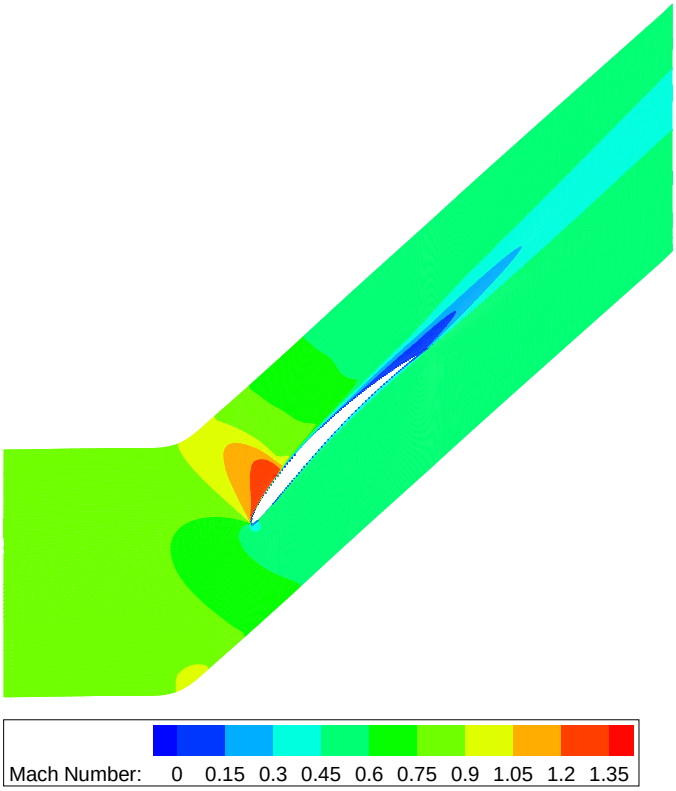

Figure 14. FLOW FIELD FOR 2D VISCOUS SIMULATION OF OFF-DESIGN CONDITION.

ing values can be seen in Figure 17.

DISCUSSION

It was shown that the corner separation predicted by the 3D viscous simulation at the design operating point caused significant differences in the steady-state and unsteady flow fields. The shape of the aerodynamic damping versus interblade phase angle for the 3D viscous simulations shown in Figure 11 is different to the shape of the plot for the 3D inviscid and 2D simulations. This difference in shape would result in significantly different aerodynamic blade influence coefficients for the 3D viscous flow compared with the 3D inviscid and 2D flows. This suggests that there is a major difference in the behavior of the unsteady waves for the 3D viscous flow.

The authors speculate that the reason for the major difference in the behavior of the unsteady waves, is the separated flow region and how the unsteady waves are transmitted and reflected in the low Mach number region. Note that local Mach number is a very important parameter in determining the behavior of unsteady wave motion.

The 3D viscous simulations did not predict large values of

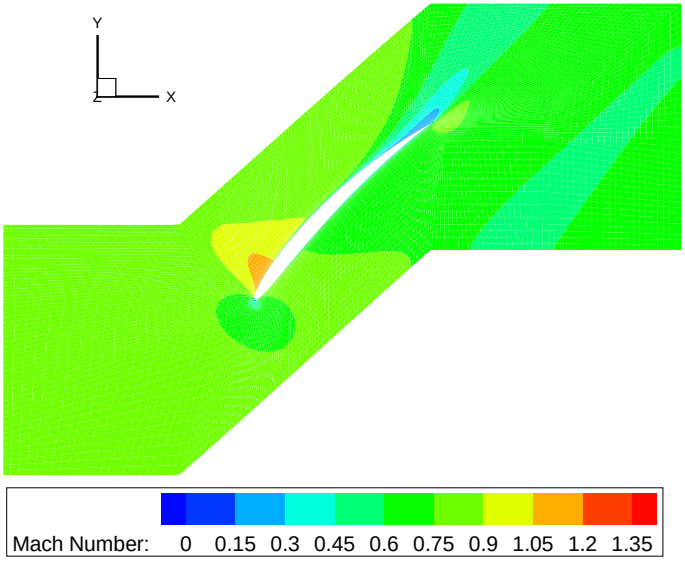

Figure 15. FLOW FIELD AT MID-RADIUS FOR 3D VISCOUS SIMULATION OF OFF-DESIGN FLOW CONDITION.

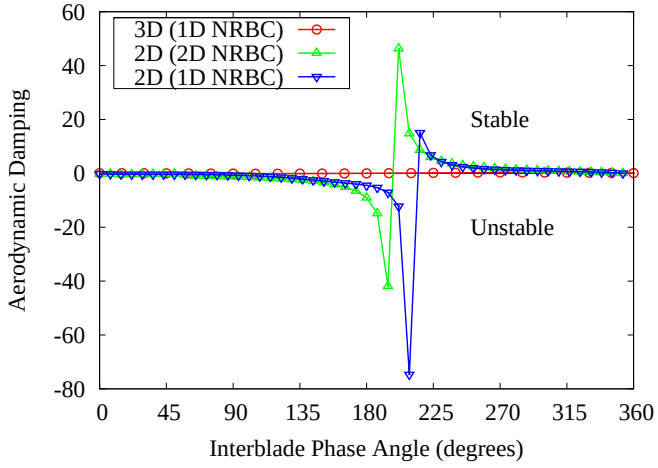

Figure 16. AERODYNAMIC DAMPING AT OFF-DESIGN FLOW CONDITION CALCULATED WITH VARIOUS VISCOUS FLOW MODELS. THE DIMENSION OF THE NON-REFLECTING BOUNDARY CONDITION IN THE FAR-FIELD IS SHOWN IN BRACKETS.

negative aerodynamic damping at the off-design operating point as were predicted by 2D viscous simulations. It can been seen by comparing Figures 14 and 15 that size and shape of the separated flow regions for the 2D viscous and 3D viscous solutions are significantly different. The authors have previously speculated [12] that the large values of negative damping predicted by the 2D

Copyright © 2007 by RPMTurbo Pty Ltd

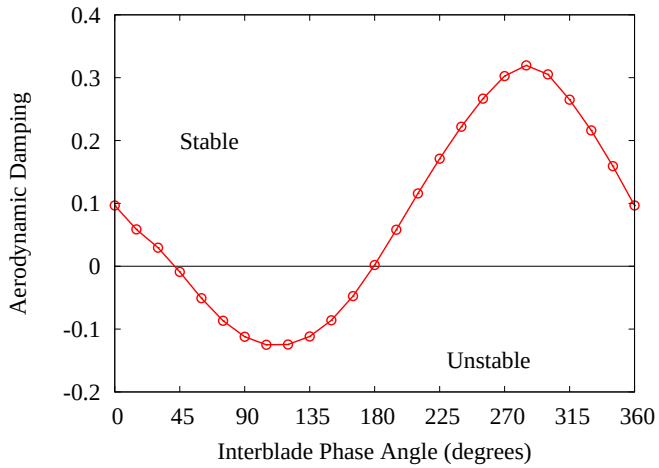

Figure 17. AERODYNAMIC DAMPING AT OFF-DESIGN FLOW CONDITION PREDICTED BY 3D VISCOUS SIMULATIONS.

viscous simulations at the off-design flow condition only occur when the separated flow region has a certain size and shape. It is further speculated here that the 3D viscous simulations do not predict large values of negative damping because of the different size and shape of the separated flow regions. This does not suggest that 3D viscous simulations will not predict large values of negative damping for all conditions. There are probably 3D flow conditions where the size and shape of the separated flow region causes near-field resonance and large values of negative aerodynamic damping, but these 3D flow conditions have not yet been discovered.

The agreement between 3D inviscid and 2D solutions for the design operating point was good. This is because the 3D inviscid simulation did not predict corner separation and the 3D inviscid flow-field was similar to the 2D flow-field.

Future Work

The authors are currently implementing an exact 3D-NRBC similar to that employed by Montgomery & Verdon [4]. It is expected that the addition of a 3D-NRBC will not change the overall conclusion of this paper, that is, 3D viscous effects are important for flutter analysis, for the cases examined here. It is expected the 3D-NRBC will affect the damping values near resonant conditions.

CONCLUSIONS

Solutions from viscous unsteady simulations of the 3D Standard Configuration 10 have been presented. The results establish a database of solutions that can be used for comparison with other numerical methods. A full description of the geometry and the steady-state and unsteady solutions for the design operation point are available for download from www.rpmturbo.com/testcases/sc10_3D.

The 3D viscous solutions were found to be significantly different from 2D and 3D inviscid simulations of Standard Configuration 10. The 3D viscous simulations predicted corner separation at the hub on the suction surface. This caused a significant flow blockage, and a lower exit pressure was required to achieve the defined inlet flow Mach number. The corner separation also had a significant effect on the unsteady flow. The 3D viscous simulations predicted negative aerodynamic damping over a large range of inter-blade phase angles for a design condition where 2D and 3D inviscid simulations predicted positive values.

An off-design test case was also examined. The 2D viscous simulations predicted large values of negative damping for this case, however, the 3D viscous simulations did not. The difference is probably due to the different size and shape of the separated flow region.

ACKNOWLEDGMENT

The simulations reported in this paper were performed on the cluster computer facility at the Centre for Hypersonics, University of Queensland. We thank the Queensland State Government and SUN Microsystems for sponsoring the development of this facility. We also thank Rowan Gollan, Andrew Denman and Marlies Hankel for the setup and maintenance of the cluster.

REFERENCES

[1] Kielb, R. E., 1998. “Unsteady flows - an aeroelastic blade design perspective”. In ERCOFTAC Turbomachinery Seminar and Workshop, Aussois, France.

[2] Srinivasan, A., 1997. “Flutter and resonant vibration characteristics of engine blades”. *Journal of Engineering for Gas Turbines and Power*, **119**, pp. 741–775.

[3] Frannson, T. H., and Verdon, J. M., 1991. Update report on standard configurations for unsteady flow through vibrating axial-flow turbomachine cascades. Progress report, Royal Institute of Technology, Stockholm, Sweden, July. URL: http://www.energy.kth.se/index.asp?pnr=10&ID=274.

[4] Montgomery, M. D., and Verdon, J. M., 1997. A three-dimensional linearized unsteady Euler analysis for turbomachinery blade rows. Contractor Report 4770, National Aeronautics and Space Administration, U.S.A.

[5] Kemme, R., 2004. “Numerische Untersuchungen zum aeroelastischen Verhalten eines hochbelasteten Verdichterrotors”. PhD thesis, German Aerospace Center (DLR).

[6] Poli, F., Gambini, E., Arnone, A., and Schipani, C., 2006. “A three-dimensional time-linearized method for turbomachinery blade flutter analysis”. In Proceedings of the

Copyright © 2007 by RPMTurbo Pty Ltd

11th International Symposium of Unsteady Aerodynamics Aeroacoustics and Aeroelasticity of Turbomachines, CIAM, Moscow, Russia.

[7] Vogt, D., 2005. "Experimental investigation of three-dimensional mechanisms in low-pressure turbine flutter". PhD thesis, Royal Institute of Technology, Stockholm, Sweden.

[8] Rzadkowski, R., Gnesin, V., and Kolodyazhnaya, L., 2006. "3D viscous flutter in turbomachinery cascade by Godunov-Kolgan method". In Proceedings of ASME TURBO EXPO. GT2006-90157.

[9] Clark, W. S., and Hall, K. C., 2000. "A time-linearized Navier-Stokes analysis of stall flutter". *Journal of Turbomachinery*, **122**, pp. 467–476.

[10] Sbardella, L., and Imregun, M., 2001. "Linearised unsteady viscous turbomachinery flows using hybrid grids". *Journal of Turbomachinery*, **123**, pp. 568–582.

[11] Spalart, P. R., and Allmaras, S. R., 1992. "A one-equation turbulence model for aerodynamic flows". In Proceedings of 30th Aerospace Sciences Meeting & Exhibit. AIAA-92-0439.

[12] Petrie-Repar, P. J., McGhee, A. M., Jacobs, P. A., and Gollan, R., 2006. "Analytical maps of aerodynamic damping as a function of operating condition for a compressor profile". In Proceedings of ASME TURBO EXPO. GT2006-90829.

[13] Giles, M., 1990. "Non-reflecting boundary conditions for the Euler calculations". *AIAA Journal*, **28**, pp. 2050–2058.

Copyright © 2007 by RPMTurbo Pty Ltd